Title: Polychlorinated biphenyl quinone-induced signaling transition from autophagy to apoptosis is regulated by HMGB1 and p53 in human hepatoma HepG2 cells

Authors: Qiong Shi, Yawen Wang, Wenjing Dong, Erqun Song, Yang Song

PII: S0378-4274(19)30034-7
DOI: https://doi.org/10.1016/j.toxlet.2019.02.002
Reference: TOXLET 10412

To appear in: *Toxicology Letters*

Received date: 16 October 2018
Revised date: 20 January 2019
Accepted date: 6 February 2019

Please cite this article as: Shi Q, Wang Y, Dong W, Song E, Song Y, Polychlorinated biphenyl quinone-induced signaling transition from autophagy to apoptosis is regulated by HMGB1 and p53 in human hepatoma HepG2 cells, *Toxicology Letters* (2019), https://doi.org/10.1016/j.toxlet.2019.02.002

Polychlorinated biphenyl quinone-induced signaling transition from autophagy to apoptosis is regulated by HMGB1 and p53 in human hepatoma HepG2 cells

Qiong Shi, Yawen Wang, Wenjing Dong, Erqun Song, Yang Song* songyangwenrong@hotmail.com

Key Laboratory of Luminescence and Real-Time Analytical Chemistry (Southwest University), Ministry of Education, College of Pharmaceutical Sciences, Southwest University, Chongqing, People's Republic of China, 400715

*Corresponding author: College of Pharmaceutical Sciences, Southwest University, Beibei, Chongqing, People's Republic of China, 400715. Tel: +86-23-68251503. Fax: +86-23-68251225

AUTHOR INFORMATION

Corresponding author

*Tel: +86-23-68251503. Fax: +86-23-68251225. E-mail address: songyangwenrong@hotmail.com or ysong@swu.edu.cn

Highlights

- PCB quinone metabolite elicited both autophagy and apoptosis.
- Relocation of ATG5 and Beclin1 suggested autophagy-to-apoptosis signaling.
- HMGB1 and p53 regulate PCB quinone-induced autophagy and apoptosis.

ABSTRACT

Autophagy, which works to remove stress and maintain cellular homeostasis, is usually considered a "pro-survival" signal. Contrarily, apoptosis is programmed "pro-death" machinery. Polychlorinated biphenyls (PCBs) are a group of ubiquitous industrial pollutants. Our previous studies illustrated that a PCB quinone metabolite, PCB29-pQ, elicited both autophagy and apoptosis. However, the signaling underlying the autophagy and apoptosis cross-talk has not been characterized. Here, we found that PCB29-pQ-induced autophagy mainly occurred at a lower concentration (5 μM), while apoptosis mostly arose at a higher concentration (15 μM) in HepG2 cells. Next, we demonstrated the elevation of intracellular calcium levels and calpain activity with PCB29-pQ treatment; however, the unaffected subcellular location of truncated ATG5 and Beclin1 suggested the irrelevance of calpain towards the autophagy-to-apoptosis signaling shift. HMGB1 and p53 both serve as transcription factors that play crucial roles in the regulation of PCB29-pQ-induced autophagy and apoptosis. PCB29-pQ not only enhanced the expression of HMGB1 and p53 but also promoted their binding and cytosolic translocation. Interestingly, HMGB1 rather than p53 plays a primary role in 5 μM of PCB29-pQ-induced autophagy in the nucleus; however, p53 promoted apoptosis to a great extent in the cytosol at the dose of 15 μM PCB29-pQ. Together, HMGB1 and p53 provided a subtle balance between autophagy and apoptosis, thus determining the fate of PCB29-pQ-treated cells.

Abbreviations

ATG5, autophagy specific gene 5; Bak, Bcl-2-antagonist/killer; Bax, Bcl-2 associated X protein; Bcl-2, B-cell lymphoma-2; Cyt c, cytochrome c; DRAM, damage-regulated autophagy modulator; HMGB1, high mobility group box 1; HSPB1, heat shock protein family B (small) member 1; LC3B, light chain 3B; MMP, mitochondrial membrane potential; PCBs, polychlorinated biphenyls; PI3K, phosphoinositide 3-kinase; RAGE, receptor for advanced glycation end products; TUNEL, terminal deoxynucleotidyl transferase (TdT)-mediated dUTP nick end labeling; ULK1, unc-51 like autophagy activating kinase 1

Keywords: PCBs; autophagy; apoptosis; HMGB1; p53

1. INTRODUCTION

Polychlorinated biphenyls (PCBs) are a series of persistent organic pollutants that have been widely distributed throughout the environment, even after being banned for more than thirty years. PCBs bio-accumulate and bio-amplify through the food chain and eventually reach considerable levels in the human body. PCBs even transfer to human embryos through the placenta and to infants through mother's milk (Safe, 1994). Recently, there has been growing concern about the adverse effects of PCBs. Numerous PCB-related toxicities have been documented, including endocrine toxicity, neurotoxicity, immunotoxicity, and genotoxicity (Crinnion, 2011; Robertson and Hansen, 2001).

Due to different numbers and positions of chlorination for each PCB congener, their antagonism towards chemical and biological metabolism are various. In general, highly chlorinated PCBs are more stable, while low chlorinated PCBs are metabolized relatively quickly. Recently, Grimm *et al* summarized the metabolic pathways and corresponding metabolites of polychlorinated biphenyls (Grimm et al., 2015). Hydroxylated polychlorinated biphenyls (OH-PCBs), which are produced by oxidative transformation of parent PCBs, are the most abundant metabolites (Tehrani and Van Aken, 2014). Indeed, OH-PCBs have been detected in wildlife, air, water and sediments at levels comparable to the parent PCBs (Eguchi et al., 2012; Tehrani and Van Aken, 2014; Weiss et al., 2006). Of note, the toxic mechanisms of the individual PCB metabolites remain poorly understood. Interestingly, growing evidence has shown that PCB metabolites, *e.g.*, OH-PCBs, exert stronger toxic effects than their parent PCBs (Bhalla et al., 2016; Montano et al., 2013; Ptak et al., 2010).

Recently, our group has been devoted to disclosing the toxicities of a further oxidized form of OH-PCBs, namely, PCB quinones. The existing data demonstrated that PCB quinones mediate multiple cellular signaling pathways. For instance, PCB quinone induces mitochondrial- (intrinsic) death receptor- (extrinsic) (Song et al., 2015) and endoplasmic reticulum-related apoptosis (Xu et al., 2015b). Interestingly, PCB quinone also triggers autophagy (Doll et al., 2016). The general function of autophagy is to remove stress and maintain cellular homeostasis, usually being considered a "pro-survival" signaling. However, severe autophagy may lead to a pro-death response; therefore autophagy is classified as a type II programmed cell death (Debnath et al., 2005; Gozuacik and Kimchi, 2004). Recently, accumulating evidence has illustrated that autophagy and apoptosis signaling might communicate with each other and exhibit mutual inhibition (Baehrecke, 2005; Maiuri et al., 2007; Marino et al., 2014; Mukhopadhyay et al., 2014). Notably, autophagy and

apoptosis can be detected under the same stress conditions, which implies that autophagy and apoptosis have common regulators (Maiuri et al., 2007). To this end, we sought to define the molecule(s) controlling autophagy and apoptosis in PCB quinone-challenged cells.

2. MATERIALS AND METHODS

2.1 Materials and Reagents

2,3,5-Trichloro-6-phenyl-[1,4]-benzoquinone (PCB29-pQ, structure shown in **Table of Content**) was synthesized and characterized following our previous method (Song et al., 2008). A mitochondrial membrane potential (MMP) assay kit with JC-1, a one-step terminal deoxynucleotidyl transferase (TdT)-mediated dUTP nick end labeling (TUNEL) apoptosis assay kit, protein A+G agarose and pifithrin-α were purchased from Beyotime Institute of Biotechnology (Nanjing, China). Rabbit Bcl-2-antagonist/killer 1 (Bak), Bcl-2 associated X protein (Bax), B-cell lymphoma-2 (Bcl-2), caspase 9, cytochrome c (Cyt c), Beclin1, and damage-regulated autophagy modulator (DRAM) polyclonal primary antibodies were obtained from Wanleibio (Shenyang, China). Rabbit autophagy specific gene 5 (ATG5), light chain 3B (LC3B), cleaved caspase 3, calpain, COX-IV, Lamin B, p53, mouse p53 primary antibodies and Alexa Fluor 488-labeled goat antimouse/antirabbit IgG (H+L) were obtained from Proteintech Group, Inc. (Wuhan, China). Rhodamine (TRITC)-conjugated AffiniPure goat anti-rabbit IgG (H+L) was supplied by ZSGB-BIO (Beijing, China). Anti-high mobility group box 1 (HMGB1) rabbit polyclonal antibody was purchased from Bioss Biotech Co. Ltd. (Beijing, China). Rabbit unc-51 like autophagy activating kinase 1 (ULK1), heat shock protein family B (small) member 1 (HSPB1) and β-actin antibodies, Goat anti-rabbit IgG HRP-conjugated secondary antibody, a cytosolic/mitochondrial protein extraction kit and a nucleoprotein extraction

kit were supplied by Sangon Biotech Company, Ltd. (Shanghai, China). 1,2-Bis(2-amino-phenoxy) ethane-N, N, N, N-tetraacetic acid (BAPTA-AM, Ca^{2+} chelator) was obtained from TCI Chemical Industry Development Co. Ltd. (Shanghai, China). Fluo-3 AM was obtained from Fanbo Biochemicals (Beijing, China). Suc-LLVY-AMC was obtained from Boston Biochem Inc. (Cambridge, MA). PD151746 (calpain inhibitor) was obtained from Selleck (Shanghai, China). Ethyl pyruvate (EP, HMGB1 inhibitor) was purchased from Aladdin Reagent Database Inc. (Shanghai, China). p53 and HMGB1 siRNAs and siRNA-mate transfection reagent were supplied by GenePharma Co., Ltd. (Shanghai, China). Dulbecco's modified Eagle's medium (DMEM) was purchased from Nanjing KeyGEN Biotech. Co., Ltd. (Nanjing, China) and fetal bovine serum was purchased from Hangzhou Sijiqing Biological Engineering Materials Co., Ltd. All other chemicals used were of the highest commercial grade.

2.2 Cell Culture and Treatment

Human hepatoma HepG2 cells were purchased from Nanjing KeyGEN Biotech. Co., Ltd. Cells were cultured in DMEM containing 10% fetal bovine serum, 100 U/mL penicillin and 100 μg/mL streptomycin at 37°C in a 5% CO_2 incubator. Cells were treated with different concentrations of PCB29-pQ.

2.3 Cell Viability

Cell viability was determined by CCK-8 according to the manufacturer's instruction. Briefly, HepG2 cells were seeded in 96-well culture plates at 10^4 cells/well. The cells were adhered overnight and exposed to a designed concentration of PCB29-pQ. Then, the medium was removed from each

well, and CCK-8 solution was added. After 3 h incubation, the optical density (OD) value was recorded at 450 nm using a microplate reader (BioTek ELX800, Vermont).

2.4 Assay for MMP

HepG2 cells were seeded into 6-well plates at 3×10^5 cells/mL with 2 mL of medium and cultivated for 24 h to adhere. After treatment with PCB29-pQ for 24 h, the cells were stained with JC-1 staining solution (5 mg/mL) at 37°C for 20 min. Then, they were washed twice with JC-1 staining buffer (1x) and added to 2 mL medium without serum. Finally, the cells were observed immediately under a fluorescence microscope (Olympus IX71). In addition, MMP fluorescence intensity was measured by a fluorescence spectrophotometer (HITACHI F-7000) at E_x/E_m=490/530 nm (JC-1 monomer) and at E_x/E_m=525/590 nm (JC-1 aggregate).

2.5 Protein Extraction

HepG2 cells were seeded into a dish (60 mm) at 10^6 cells/ml with 5 mL of medium and cultivated for 24 h to adhere, and after being treated with PCB29-pQ, the cells were washed twice with PBS and lysed with RIPA lysis buffer for 30 min. The cell lysate was collected by centrifugation at 10,000 g at 4°C for 10 min for total protein extraction. Corresponding kits were used for cytosolic/mitochondrial or cytosolic/nuclear protein extraction according to the manufacturer's instructions. The concentration of protein was tested by Bradford Protein Assay Kit (Nanjing Jiancheng Institute of Biotechnology, Nanjing, China).

2.6 Co-immunoprecipitation (Co-IP)

HepG2 cells were seeded into a dish (100 mm) at 6×10^6 cells/ml with 10 mL of medium and cultivated for 24 h to adhere. After being treated with PCB29-pQ, cells were lysed with RIPA buffer and collected by centrifugation at 10,000 g for 10 min. Two micrograms of p53 or HMGB1 antibody was added to approximately 1 mg of the cell lysate. Then, Protein A+G agarose was used to resuspend with the lysate at 4°C overnight. The mixture was centrifuged at 2,500 g for 5 min, and the pelleted agarose was washed five times with PBS at 2,500 g for 5 min. Next, the sample was resuspended in 40 μL loading buffer and heated at 97°C for 10 min. Then, the sample was centrifuged at 2,500 g for 5 min, and the supernatant was collected for Western blotting analysis.

2.7 Western Blotting Analysis

Samples were separated by 10% or 12.5% SDS-PAGE, transferred onto nitrocellulose membranes and blocked in 5% nonfat dry milk at 37°C for 1.5 h. Then, the membranes were incubated with primary antibodies at 4°C overnight or 37°C 3 h. After washing in TBST three times, the membranes were incubated with appropriate secondary antibodies conjugated to horseradish peroxidase at 37°C for 2 h. Finally, the proteins were visualized using the ECL system (Beyotime Biotechnology, Shanghai, China).

2.8 Immunofluorescence Staining

HepG2 cells were plated onto confocal dishes and cultured to adhere at 37°C and 5% CO_2. After being treated with PCB29-pQ, the cells were washed with PBS, fixed in 4% paraformaldehyde for 30 min and permeabilized with 1% Triton X-100 for 20 min. After blocking with 10% BSA at 4°C for 1 h, cells were incubated with primary rabbit LC3B at 4°C overnight and then incubated with

Alexa Fluor 488-labeled goat anti-rabbit IgG (H+L) for 1 h. Alternatively, cells were incubated with primary rabbit HMGB1 antibody and mouse p53 antibody at 4°C overnight, then, they were incubated with secondary antibody, Alexa Fluor 488-labeled goat anti-mouse IgG (H+L) and Rhodamine (TRITC)-conjugated AffiniPure goat anti-rabbit IgG (H+L) at 37°C for 1 h. Finally, the cells were analyzed with a fluorescence microscope (OLYMPUS IX71).

2.9 TUNEL Assay

After treating with PCB29-pQ, cells were washed with PBS, fixed in 4% paraformaldehyde for 30 min, and permeabilized with 0.1% Triton X-100 on ice for 2 min. Then, 50 μL TUNEL test solution was added, and incubated at 37°C for 60 min in dark. Cells were washed in PBS three times, then they were analyzed with a fluorescence microscope (OLYMPUS IX71).

2.10 Intracellular Calcium Level Measurement

Calcium levels were determined using Fluo-3 AM fluorescent probe. HepG2 cells attached to 6-well plates to adhere; then, the cells were treated with PCB29-pQ for 24 h and washed with PBS. The cells were cultured for an additional 1 h in serum-free medium containing Fluo-3 AM (final concentration of 2 μM). Then, the cells were washed once with PBS, cultured in serum-free medium for another 20 min, and detected by BD FACS Vantage SE flow cytometer (BD Biosciences). Data were analyzed using BD Cell Quest software.

2.11 Calpain Activity Measurement

Calpain activity was determined using S-LLVY-AMC as a cell-permeable fluorogenic calpain substrate. HepG2 cells were treated with PCB29-pQ and harvested with 0.25% trypsin-EDTA solution. Then, the cells were resuspended in PBS at 3×10^6 cells/mL. The sample was incubated in a 96-well plate by adding 25 μM S-LLVY-AMC at 37℃ for 15 min. The AMC fluorescence intensity was measured in a HITACHI F7000 fluorescence spectrophotometer with an excitation wavelength of 351 nm and an emission wavelength of 430 nm.

2.12 Small RNA (siRNA) Interference

HepG2 cells were transfected with negative control siRNA, p53 siRNA or HMGB1 siRNA at 50 nM using siRNA-mate transfection reagent for 24 h, according to the manufacturer's instructions. The sequences for siRNA targeting were as follows: p53 sense, 5′-GGA AGA CUC CAG UGG UAA UTT-3′; p53 antisense, 5′-AUU ACC ACU GGA GUC UUC CAG-3′. HMGB1 sense, 5′-CAG GAG GAA UAC UGA ACA U-3′; HMGB1 antisense, 5′-AUG UUC AGU AUU CCU CCU G-3′. Calpain sense, 5′-GCU UUU GUU CUC UCA GUA CTT-3′; Calpain antisense, 5′-GUA CUG AGA GAA CAA AAG CTT-3′. Then, cells were incubated in 10% serum medium for 24 h followed by PCB29-pQ exposure for an additional 24 h.

2.13 Flow Cytometry Analysis

HepG2 cells were treated with PCB29-pQ and harvested with 0.25% trypsin-EDTA solution. The cells were resuspended with PBS and incubated with FITC-conjugated annexin-V/propidium iodide (PI) double staining solution for 15 min according to the manufacturer's instructions.

Fluorescence was determined on a BD FACS Vantage SE flow cytometer (BD Biosciences), and the percentage of apoptotic cells was calculated using BD Cell Quest software.

2.14 Statistical Analysis

Data were shown as the mean ± standard deviation (SD). Statistical significance was determined by one-way analysis of variance (ANOVA) followed by least significance difference (LSD) multiple comparison tests using SPSS19 software. $P < 0.05$ was considered significant.

3. RESULTS AND DISCUSSION

3.1 Autophagy-To-Apoptosis Signaling Switch *via* Increasing Concentration of PCB29-pQ

The HepG2 cell line was originally derived from a human hepatoblastoma and retains many of the functions of normal liver cells, and it has been used in our previous studies (Doll et al., 2016; Xu et al., 2015b). To achieve evidence of a PCB29-pQ-induced autophagy-to-apoptosis signaling switch, cells were treated with 5 to 20 μM of PCB29-pQ for 24 h. The choice of the concentration and duration of PCB29-pQ is based on our previous publication (Doll et al., 2016; Dong et al., 2014; Song et al., 2015; Xu et al., 2015a).

First, MMP was monitored using the JC-1 probe; the control group and 5 μM group showed orange fluorescence indicating an intact outer mitochondrial membrane, while green fluorescence took over after higher concentration PCB29-pQ treatment (10 μM and beyond) indicating compromised membrane integrity, **Figure 1A**. To further study the effect of PCB29-pQ-induced apoptosis, the expression of apoptosis-related factors was measured by Western blotting. Cyt c is released from mitochondria into cytosol through damaged membrane and activates downstream

caspase cascades (Pham et al., 2016). Along with the increased Cyt c, PCB29-pQ treatment increased Bax and Bak expression and decreased that of Bcl-2, **Figure 1B**. Furthermore, the cleavage forms of caspase 9 and caspase 3 were significantly increased. PCB29-pQ-induced autophagy was detected by measuring the number of LC3 puncta using an immunofluorescence assay. As shown in **Figure 1C**, the maximum number of LC3 puncta was found in the 5 μM PCB29-pQ group. This result is consistent with our previous study in which 5 μM PCB29-pQ caused the highest acridine orange positive cell number, monodansylcadaverine staining, LC3 mRNA level and LC3B net flux in two unrelated cell lines (Doll et al., 2016). For a direct comparison, TUNEL results showed increased red fluorescence at higher concentrations (10 and 15 μM groups), which implied the existence of apoptosis. Based on these results, we concluded that PCB29-pQ induced autophagy at lower concentrations and shifted to apoptosis at high concentrations.

3.2 Intracellular Calcium Level and Calpain Activity Were Induced by PCB29-pQ but Made No Contribution to Autophagy-To-Apoptosis Shift

Next, we ought to address the transition mechanism from autophagy to apoptosis. ATG5 is involved in the process of autophagosome formation; Beclin1 (a mammalian ortholog of ATG6) is required for autophagosome initiation and autophagosome closure. Alternatively, they may also play a role in a pro-apoptotic pathway (Yousefi et al., 2006; Yousefi and Simon, 2007). ATG5 and Beclin1 are cleaved by calpain, turning to pro-apoptotic truncation products tATG5 and Beclin1-c (Lepine et al., 2011; Shi et al., 2013; Yousefi et al., 2006). The calpains are a group of well-conserved calcium-sensitive proteases, ubiquitously expressed in cells. Cytosolic Ca^{2+} is a stimulator of calpains that links with autophagy or apoptosis. Increased cytosolic Ca^{2+} causes mitochondria

overload and constitutes a prominent pro-apoptotic signal (Rizzuto and Pozzan, 2006). Additionally, cytosolic Ca^{2+} activates calmodulin-dependent kinase kinase-β, which inhibits mTOR and amplifies autophagy (Hoyer-Hansen et al., 2007). We previously demonstrated that PCB29-pQ elevated intracellular Ca^{2+} levels and calpain activity, which effects were abrogated by the Ca^{2+} chelator BAPTA-AM (Xu et al., 2015b). In **Figure 2A**, PCB29-pQ increased the intracellular Ca^{2+} level in a concentration-dependent manner, and significant differences were found in the 15 and 20 μM groups ($p<0.001$). This promotion was significantly inhibited by pretreatment with BAPTA-AM. As illustrated in **Figure 2B**, as the PCB29-pQ concentration increased, the fluorescence intensity of AMC from calpain cleavage was significantly enhanced and a peak appeared at ~430 nm. A corresponding histogram of fluorescence intensity versus concentration of PCB29-pQ is also presented. PCB29-pQ significantly increased the activity of calpain, compared with the control group. In addition, the protein expression of calpain was tested by Western blotting analysis in **Figure 2C**; PCB29-pQ up-regulated the expression of calpain, and BAPTA-AM reversed this effect. This result proved that PCB29-pQ-induced calpain expression was dependent on intracellular Ca^{2+} level. Of note, the effect of BAPTA-AM was found with higher concentration of PCB29-pQ treatment groups (**Figure 2A** and **2C**), suggested this effect is somehow related to more severe damages. However, these results were insufficient to conclude that the signal switch of autophagy-to-apoptosis is linked to elevated calcium levels and calpain activity.

After the N-terminal fragment (BCL-2-binding domain) is removed, the C-terminal fragments of Beclin1 translocate to mitochondria and turn into a pro-apoptotic protein that induces Cyt c release (Djavaheri-Mergny et al., 2010). Similarly, N-terminal tAtg5 triggers Cyt c release from mitochondria. Thus, the translocation of cleaved products is essential for their pro-apoptotic

function. We checked whether PCB29-pQ induces the cleavage/mitochondrial translocation of ATG5 and Beclin1. Since only higher concentrations (>=15 μM) of PCB29-pQ exposure cause significant apoptosis (result from **Figure 1**) and 20 μM of PCB29-pQ causes unwanted cytotoxicity, cell viability <50%, result from our previous publication (Doll et al., 2016; Dong et al., 2014), we therefore mainly chose a concentration of 15 μM for further experiments. We extracted mitochondrial and cytosolic proteins to check the distribution of ATG5 and Beclin1. We found the cleaved ATG5 and Beclin1 after PCB29-pQ (15 μM) exposure; however, they do not present in the mitochondrial fraction, **Figure 3A**.

Calpain is involved in the apoptotic process at different steps (Wu et al., 2014). We previously illustrated that PCB29-pQ-increased calpain activity was inhibited by BAPTA-AM (Ca^{2+} chelator) (Xu et al., 2015b). Here, however, neither BAPTA-AM, PD151746 (calpain inhibitor) nor calpain siRNA treatment showed any significant effect on the loss of viability induced by 15 μM PCB29-pQ, **Figure 3B**. Flow cytometry also showed parallel results, **Figure 3C**. Together, we speculated that calpain is irrelevant to the PCB29-pQ (15 μM)-induced autophagy-to-apoptosis signal switch.

3.3 PCB29-pQ Induced p53 and HMGB1 Cytosolic Translocation and Increased HMGB1/p53 Binding

p53 and HMGB1 play crucial roles in the regulation of apoptosis/autophagy balance (Livesey et al., 2012). p53 promotes apoptosis through transcription-dependent and transcription-independent mechanisms (Chipuk et al., 2005; Chipuk et al., 2004). In contrast, p53 shows both positive and negative functions in the regulation of autophagy, depending on its subcellular location. Cytosolic p53 represses autophagy in a transcription-independent fashion (Tasdemir et al., 2008), while nuclear

p53 stimulates autophagy transcription-dependently (Crighton et al., 2006; Gao et al., 2011). HMGB1 is a highly conserved nuclear protein; after being released, it serves as an extracellular mediator in various pathological and stress conditions, *e.g.*, inflammation, cell differentiation and migration (Lotze and Tracey, 2005) Tang *et al* showed that HMGB1 promotes autophagy both transcription-dependently and –independently (Tang et al., 2010; Tang et al., 2011). To be specific, cytosolic HMGB1 binds with Beclin1 and maintains the activation of Beclin1/phosphoinositide 3-kinase (PI3K) complex,(Tang et al., 2010) whereas exogenous HMGB1 interacts with receptor for advanced glycation end products (RAGE) (Kang et al., 2011; Kang et al., 2010). In addition, p53 and HMGB1 form a complex that regulates the level of autophagy (Livesey et al., 2012). We first detected the expression of p53 and HMGB1 proteins after PCB29-pQ stimulation. As shown in **Figure 4A**, after cells were treated with PCB29-pQ for 24 h, the expression of p53 and HMGB1 proteins was gradually enhanced. To study the effect of different subcellular localization of p53 and HMGB1 on the autophagy-to-apoptosis signal switch, we detected corresponding protein levels in the cytosol and nucleus, separately. In In **Figure 4B and C**, the protein expressions of p53 and HMGB1 were increased in the cytosol but decreased in the nucleus and at both concentrations, compare with the control (5 and 15 μM). This result was further confirmed by immunofluorescence staining, which suggested that PCB29-pQ promoted the transfer of p53 and HMGB1 from the nucleus to the cytosol, **Figure 4D**. p53 and HMGB1 were localized in nucleus mainly when treated with 5 μM dose of PCB29-pQ. Moreover, they were localized in cytosol mainly when treated with 15 μM dose of PCB29-pQ.

To validate the interaction between p53 and HMGB1, we immunoprecipitated whole cell lysates with HMGB1 or p53 antibody and probed for the reciprocal target protein, as shown in

Figure 4E and F. The amounts of loading protein on the lower panel were normalized for comparison, thus the increased p53 (or HMGB1) immunoblotting indicated PCB29-pQ-treatment enhanced HMGB1/p53 binding in both groups. Indeed, the interaction between p53 and HMGB1 were enhanced in total proteins at the concentration of 5- and 15uM PCB29-pQ group. Moreover, the nuclear and cytosolic proteins were extracted and analyzed for their binding efficiency in different cellular compartment. HMGB1/p53 binding was mainly in the nucleus in the 5 μM group and in the cytosol in the 15 μM group, **Figure 4G and H**. However, it is currently unknown whether the enhanced binding of HMGB1/p53 is due to the up-regulated expression of both proteins or increased binding constant of the HMGB1/p53 complex (HMGB1 has three oxidizable thiol groups and the binding constant of HMGB1/p53 depends on the redox status of HMGB1 (Livesey et al., 2012)). The abundance of cytoplasmic p53 and HMGB1 increased at the expense of their nuclear levels judged by both Western blotting and immunofluorescence staining. Again, HMGB1/p53 binding mainly in the nucleus at a low dose of PCB29-pQ and in the cytosol at a high dose. Nucleus HMGB1 and p53 limit apoptosis, whilst the cellular translocation of HMGB1 and p53 to cytosol consequently inhibits autophagy and might unleash apoptosis as well. Enhanced HMGB1/p53 binding also implied the signal shift from autophagy to apoptosis. Thus, PCB29-pQ regulates the cytoplasmic localization of the p53 and HMGB1 may be involved the transition of autophagy and apoptosis.

3.4 p53 and HMGB1 Are Closely Linked with PCB29-pQ-Induced Autophagy and Apoptosis

To further investigate the roles of p53 and HMGB1 in PCB29-pQ-induced autophagy and apoptosis, their downstream genes were blotted accordingly. DRAM and ULK1 are p53 target genes that encode lysosomal proteins and induce autophagy (Crighton et al., 2006; Gao et al., 2011). For

instance, Crighton et al demonstrated that p53 silence downregulated DRAM expression (Crighton et al., 2006). Alternatively, p53 activates its target genes (*e.g.*, Bax, Fas and Apaf-1) that induce apoptosis. In **Figure 5A**, treatment with 5 μM and 15 μM PCB29-pQ increased the expressions of DRAM, ULK1, Bax and p53 proteins (except DRAM for 15 μM) compared with control group. While incubation of cells with 15 μM PCB29-pQ, the expressions of DRAM and ULK1 proteins were progressively reduced compared to 5 μM PCB29-pQ. Therefore, PCB29-pQ could mainly elicited autophagy when used at low concentration (5 μM). In comparison, the expressions of Bax and p53 proteins were upregulation in the both concentrations, suggesting the occurrence of apoptosis and mainly eliciting apoptosis when used at high concentration (15 μM). This result suggested that p53 directly activates Bax through a non-transcriptional mechanism. To explore the influence of p53 on the autophagy-to-apoptosis signaling switch, we suppressed p53 expression by siRNA. We carefully optimize the concentration of siRNA, in order to maximum the effect of downregulation of DRAM and ULK1 by siRNA treatment upon 5 μM PCB29-pQ co-exposure. The inhibition of p53 completely abrogated this effect. HMGB1 regulates the expression of HSPB1 in the nucleus as a transcription factor that is important for autophagy (Tang et al., 2011). Similarly, in both 5 μM and 15 μM PCB29-pQ concentrations up-regulated the expression of HSPB1, then it was progressively reduced in the 15 μM PCB29-pQ group. which effect was suppressed by HMGB1 siRNA, **Figure 5B**. These results suggested that p53 and HMGB1 largely participated in PCB29-pQ-induced autophagy and apoptosis.

3.5 P53 and HMGB1 play different roles in autophagy and apoptosis in PCB29-pQ-treated cells.

We next addressed the question of how PCB29-pQ-mediated p53 and HMGB1 affect the autophagy-to-apoptosis signaling switch. Endogenous HMGB1-regulated autophagy is dependent on ROS through the force of translocation of HMGB1 from nucleus to cytosol (Tang et al., 2010), which promotes autophagy and inhibits apoptosis (Zhang et al., 2015). Again, when HepG2 cells were exposed to low dose of PCB29-pQ (e.g., 5 μM), HMGB1 and p53 remain in nuclei, whilst in the presence of high doses of PCB29-pQ (e.g., 15 μM), both proteins move to cytosol and this translocation consequently inhibits autophagy and might unleash apoptosis as well (as seen in **Figure 4B and 4C)**. In **Figure 6A**, p53 siRNA further increased PCB29-pQ-induced LC3 puncta number in both 5 and 15 μM groups, our result indicated p53 inhibited autophagy in PCB29-pQ-treated cells. Similarly, Tasdemir *et al* reported gradually increased autophagy in human $p53^{-/-}$ colon cancer cells, while the reloading of p53 attenuated the level of autophagy (Tasdemir et al., 2008). p53 promotes apoptosis through transcription-dependent in nucleus and transcription-independent mechanisms in the cytosol. There were up-regulated cell viabilities in both low dose (5 μM) and high dose (15 μM) of PCB29-pQ after p53 siRNA, compared with control siRNA group in **Figure 6B**, indicated that p53 increases apoptosis in PCB29-pQ-treated cells. Combining these results, we concluded p53 plays a role in decreasing autophagy and increasing apoptosis in PCB29-pQ-treated cells.

To further investigate the role of HMGB1 on the modulation of PCB29-pQ-induced autophagy and apoptosis, HMGB1 was abrogated through siRNA interfering. In **Figure 6C**, HMGB1 siRNA further decreased LC3 puncta number which suggesting decreased autophagy at both concentrations of PCB29-pQ exposure. This evidence verified that HMGB1 upregulates autophagy in PCB29-pQ-treated cells. Interestingly, HMGB1 siRNA has no significant effect on PCB29-pQ-mediated viability loss, **Figure 6D**. These results suggested that HMGB1 plays important role in promoted

autophagy. It is clear that PCB29-pQ elicit autophagy at 5 μM and apoptosis at 15 μM in HepG2 cells. Again, p53 plays a role in decreasing autophagy and increasing apoptosis in PCB29-pQ-treated cells. Besides, p53 remains in nuclei when exposed to 5 μM PCB29-pQ, whilst p53 remains in cytosol when exposed to 15 μM PCB29-pQ. Therefore, p53 play an important role in increasing apoptosis at 15 μM PCB29-pQ. Similarly, HMGB1 plays important role in promoted autophagy, and HMGB1 remains in nuclei when exposed to 5 μM PCB29-pQ, whilst HMGB1 remains in cytosol when exposed to 15 μM PCB29-pQ. Although we did not find appreciable effect of HMGB1 siRNA on cell viability induced by PCB29-pQ, it may have other mechanism or regulators that was not been discussed.

4. CONCLUSION

To summary, we found that PCB29-pQ induces autophagy and apoptosis at different concentrations in HepG2 cells. PCB29-pQ treatment promoted not only p53 and HMGB1 expression but also p53/HMGB1 complex binding and nucleus-to-cytosol translocation. The entire transition from autophagy to apoptosis was under the co-influence of HMGB1 and p53.

Funding

This work is supported by National Natural Science Foundation of China (21622704, 21477098 and 21575118) and Fundamental Research Funds for the Central Universities (XDJK2018AA007 and XDJK2017A017).

Notes

The authors declare no competing financial interest.

REFERENCES

Baehrecke, E.H., 2005. Autophagy: dual roles in life and death? Nat Rev Mol Cell Biol 6, 505-510.

Bhalla, R., Tehrani, R., Van Aken, B., 2016. Toxicity of hydroxylated polychlorinated biphenyls (HO-PCBs) using the bioluminescent assay Microtox((R)). Ecotoxicology 25, 1438-1444.

Chipuk, J.E., Bouchier-Hayes, L., Kuwana, T., Newmeyer, D.D., Green, D.R., 2005. PUMA couples the nuclear and cytoplasmic proapoptotic function of p53. Science 309, 1732-1735.

Chipuk, J.E., Kuwana, T., Bouchier-Hayes, L., Droin, N.M., Newmeyer, D.D., Schuler, M., Green, D.R., 2004. Direct activation of Bax by p53 mediates mitochondrial membrane permeabilization and apoptosis. Science 303, 1010-1014.

Crighton, D., Wilkinson, S., O'Prey, J., Syed, N., Smith, P., Harrison, P.R., Gasco, M., Garrone, O., Crook, T., Ryan, K.M., 2006. DRAM, a p53-induced modulator of autophagy, is critical for apoptosis. Cell 126, 121-134.

Crinnion, W.J., 2011. Polychlorinated biphenyls: persistent pollutants with immunological, neurological, and endocrinological consequences. Altern Med Rev 16, 5-13.

Debnath, J., Baehrecke, E.H., Kroemer, G., 2005. Does autophagy contribute to cell death? Autophagy 1, 66-74.

Djavaheri-Mergny, M., Maiuri, M.C., Kroemer, G., 2010. Cross talk between apoptosis and autophagy by caspase-mediated cleavage of Beclin 1. Oncogene 29, 1717-1719.

Doll, S., Proneth, B., Tyurina, Y.Y., Panzilius, E., Kobayashi, S., Ingold, I., Irmler, M., Beckers, J., Aichler, M., Walch, A., 2016. Acsl4 Dictates Ferroptosis Sensitivity by Shaping Cellular Lipid Composition. Nature Chemical Biology 13, 91-98.

Dong, H., Su, C., Xia, X., Li, L., Song, E., Song, Y., 2014. Polychlorinated biphenyl quinone-induced genotoxicity, oxidative DNA damage and gamma-H2AX formation in HepG2 cells. Chem Biol Interact 212, 47-55.

Eguchi, A., Nomiyama, K., Devanathan, G., Subramanian, A., Bulbule, K.A., Parthasarathy, P., Takahashi, S., Tanabe, S.,

2012. Different profiles of anthropogenic and naturally produced organohalogen compounds in serum from residents living near a coastal area and e-waste recycling workers in India. Environ Int 47, 8-16.

Gao, W., Shen, Z., Shang, L., Wang, X., 2011. Upregulation of human autophagy-initiation kinase ULK1 by tumor suppressor p53 contributes to DNA-damage-induced cell death. Cell Death Differ 18, 1598-1607.

Gozuacik, D., Kimchi, A., 2004. Autophagy as a cell death and tumor suppressor mechanism. Oncogene 23, 2891-2906.

Grimm, F.A., Hu, D., Kania-Korwel, I., Lehmler, H.J., Ludewig, G., Hornbuckle, K.C., Duffel, M.W., Bergman, A., Robertson, L.W., 2015. Metabolism and metabolites of polychlorinated biphenyls. Crit Rev Toxicol 45, 245-272.

Hoyer-Hansen, M., Bastholm, L., Szyniarowski, P., Campanella, M., Szabadkai, G., Farkas, T., Bianchi, K., Fehrenbacher, N., Elling, F., Rizzuto, R., Mathiasen, I.S., Jaattela, M., 2007. Control of macroautophagy by calcium, calmodulin-dependent kinase kinase-beta, and Bcl-2. Mol Cell 25, 193-205.

Kang, R., Tang, D., Livesey, K.M., Schapiro, N.E., Lotze, M.T., Zeh, H.J., 3rd, 2011. The Receptor for Advanced Glycation End-products (RAGE) protects pancreatic tumor cells against oxidative injury. Antioxid Redox Signal 15, 2175-2184.

Kang, R., Tang, D., Schapiro, N.E., Livesey, K.M., Farkas, A., Loughran, P., Bierhaus, A., Lotze, M.T., Zeh, H.J., 2010. The receptor for advanced glycation end products (RAGE) sustains autophagy and limits apoptosis, promoting pancreatic tumor cell survival. Cell Death Differ 17, 666-676.

Lepine, S., Allegood, J.C., Edmonds, Y., Milstien, S., Spiegel, S., 2011. Autophagy induced by deficiency of sphingosine-1-phosphate phosphohydrolase 1 is switched to apoptosis by calpain-mediated autophagy-related gene 5 (Atg5) cleavage. J Biol Chem 286, 44380-44390.

Livesey, K.M., Kang, R., Vernon, P., Buchser, W., Loughran, P., Watkins, S.C., Zhang, L., Manfredi, J.J., Zeh, H.J., 3rd, Li, L., Lotze, M.T., Tang, D., 2012. p53/HMGB1 complexes regulate autophagy and apoptosis. Cancer Res 72, 1996-2005.

Lotze, M.T., Tracey, K.J., 2005. High-mobility group box 1 protein (HMGB1): nuclear weapon in the immune arsenal. Nat Rev Immunol 5, 331-342.

Maiuri, M.C., Zalckvar, E., Kimchi, A., Kroemer, G., 2007. Self-eating and self-killing: crosstalk between autophagy and apoptosis. Nat Rev Mol Cell Biol 8, 741-752.

Marino, G., Niso-Santano, M., Baehrecke, E.H., Kroemer, G., 2014. Self-consumption: the interplay of autophagy and apoptosis. Nat Rev Mol Cell Biol 15, 81-94.

Montano, M., Gutleb, A.C., Murk, A.J., 2013. Persistent toxic burdens of halogenated phenolic compounds in humans and wildlife. Environ Sci Technol 47, 6071-6081.

Mukhopadhyay, S., Panda, P.K., Sinha, N., Das, D.N., Bhutia, S.K., 2014. Autophagy and apoptosis: where do they meet? Apoptosis 19, 555-566.

Pham, T.D., Pham, P.Q., Li, J., Letai, A.G., Wallace, D.C., Burke, P.J., 2016. Cristae remodeling causes acidification detected by integrated graphene sensor during mitochondrial outer membrane permeabilization. Sci Rep 6, 35907.

Ptak, A., Ludewig, G., Rak, A., Nadolna, W., Bochenek, M., Gregoraszczuk, E.L., 2010. Induction of cytochrome P450 1A1 in MCF-7 human breast cancer cells by 4-chlorobiphenyl (PCB3) and the effects of its hydroxylated metabolites on cellular apoptosis. Environ Int 36, 935-941.

Rizzuto, R., Pozzan, T., 2006. Microdomains of intracellular Ca2+: molecular determinants and functional consequences. Physiol Rev 86, 369-408.

Robertson, L.W., Hansen, L.G., 2001. Polychlorinated Biphenyls: Metabolism and Metabolites. In PCBs: Recent Advances in the Environmental Toxicology and Health Effects of PCBs. University Press of Kentucky, Lexington, KY.

Safe, S.H., 1994. Polychlorinated biphenyls (PCBs): environmental impact, biochemical and toxic responses, and implications for risk assessment. Crit Rev Toxicol 24, 87-149.

Shi, M., Zhang, T., Sun, L., Luo, Y., Liu, D.H., Xie, S.T., Song, X.Y., Wang, G.F., Chen, X.L., Zhou, B.C., Zhang, Y.Z., 2013. Calpain, Atg5 and Bak play important roles in the crosstalk between apoptosis and autophagy induced by influx of extracellular calcium. Apoptosis 18, 435-451.

Song, X., Li, L., Shi, Q., Lehmler, H.J., Fu, J., Su, C., Xia, X., Song, E., Song, Y., 2015. Polychlorinated Biphenyl Quinone Metabolite Promotes p53-Dependent DNA Damage Checkpoint Activation, S-Phase Cycle Arrest and Extrinsic Apoptosis in Human Liver Hepatocellular Carcinoma HepG2 Cells. Chem Res Toxicol 28, 2160-2169.

Song, Y., Buettner, G.R., Parkin, S., Wagner, B.A., Robertson, L.W., Lehmler, H.J., 2008. Chlorination increases the persistence of semiquinone free radicals derived from polychlorinated biphenyl hydroquinones and quinones. J Org Chem 73, 8296-8304.

Tang, D., Kang, R., Livesey, K.M., Cheh, C.W., Farkas, A., Loughran, P., Hoppe, G., Bianchi, M.E., Tracey, K.J., Zeh, H.J., 3rd, Lotze, M.T., 2010. Endogenous HMGB1 regulates autophagy. J Cell Biol 190, 881-892.

Tang, D., Kang, R., Livesey, K.M., Kroemer, G., Billiar, T.R., Van Houten, B., Zeh, H.J., 3rd, Lotze, M.T., 2011. High-mobility group box 1 is essential for mitochondrial quality control. Cell Metab 13, 701-711.

Tasdemir, E., Maiuri, M.C., Galluzzi, L., Vitale, I., Djavaheri-Mergny, M., D'Amelio, M., Criollo, A., Morselli, E., Zhu, C., Harper, F., Nannmark, U., Samara, C., Pinton, P., Vicencio, J.M., Carnuccio, R., Moll, U.M., Madeo, F., Paterlini-Brechot, P., Rizzuto, R., Szabadkai, G., Pierron, G., Blomgren, K., Tavernarakis, N., Codogno, P., Cecconi, F., Kroemer, G., 2008. Regulation of autophagy by cytoplasmic p53. Nat Cell Biol 10, 676-687.

Tehrani, R., Van Aken, B., 2014. Hydroxylated polychlorinated biphenyls in the environment: sources, fate, and toxicities. Environ Sci Pollut Res Int 21, 6334-6345.

Weiss, J., Wallin, E., Axmon, A., Jonsson, B.A., Akesson, H., Janak, K., Hagmar, L., Bergman, A., 2006. Hydroxy-PCBs, PBDEs, and HBCDDs in serum from an elderly population of Swedish fishermen's wives and associations with bone density. Environ Sci Technol 40, 6282-6289.

Wu, H., Che, X., Zheng, Q., Wu, A., Pan, K., Shao, A., Wu, Q., Zhang, J., Hong, Y., 2014. Caspases: a molecular switch node in the crosstalk between autophagy and apoptosis. Int J Biol Sci 10, 1072-1083.

Xu, D., Li, L., Liu, L., Dong, H., Deng, Q., Yang, X., Song, E., Song, Y., 2015a. Polychlorinated biphenyl quinone induces

mitochondrial-mediated and caspase-dependent apoptosis in HepG2 cells. Environ Toxicol 30, 1063-1072.

Xu, D., Su, C., Song, X., Shi, Q., Fu, J., Hu, L., Xia, X., Song, E., Song, Y., 2015b. Polychlorinated biphenyl quinone induces endoplasmic reticulum stress, unfolded protein response, and calcium release. Chem Res Toxicol 28, 1326-1337.

Yousefi, S., Perozzo, R., Schmid, I., Ziemiecki, A., Schaffner, T., Scapozza, L., Brunner, T., Simon, H.U., 2006. Calpain-mediated cleavage of Atg5 switches autophagy to apoptosis. Nat Cell Biol 8, 1124-1132.

Yousefi, S., Simon, H.U., 2007. Apoptosis regulation by autophagy gene 5. Crit Rev Oncol Hematol 63, 241-244.

Zhang, L., Wang, K., Lei, Y., Li, Q., Nice, E.C., Huang, C., 2015. Redox signaling: Potential arbitrator of autophagy and apoptosis in therapeutic response. Free Radic Biol Med 89, 452-465.

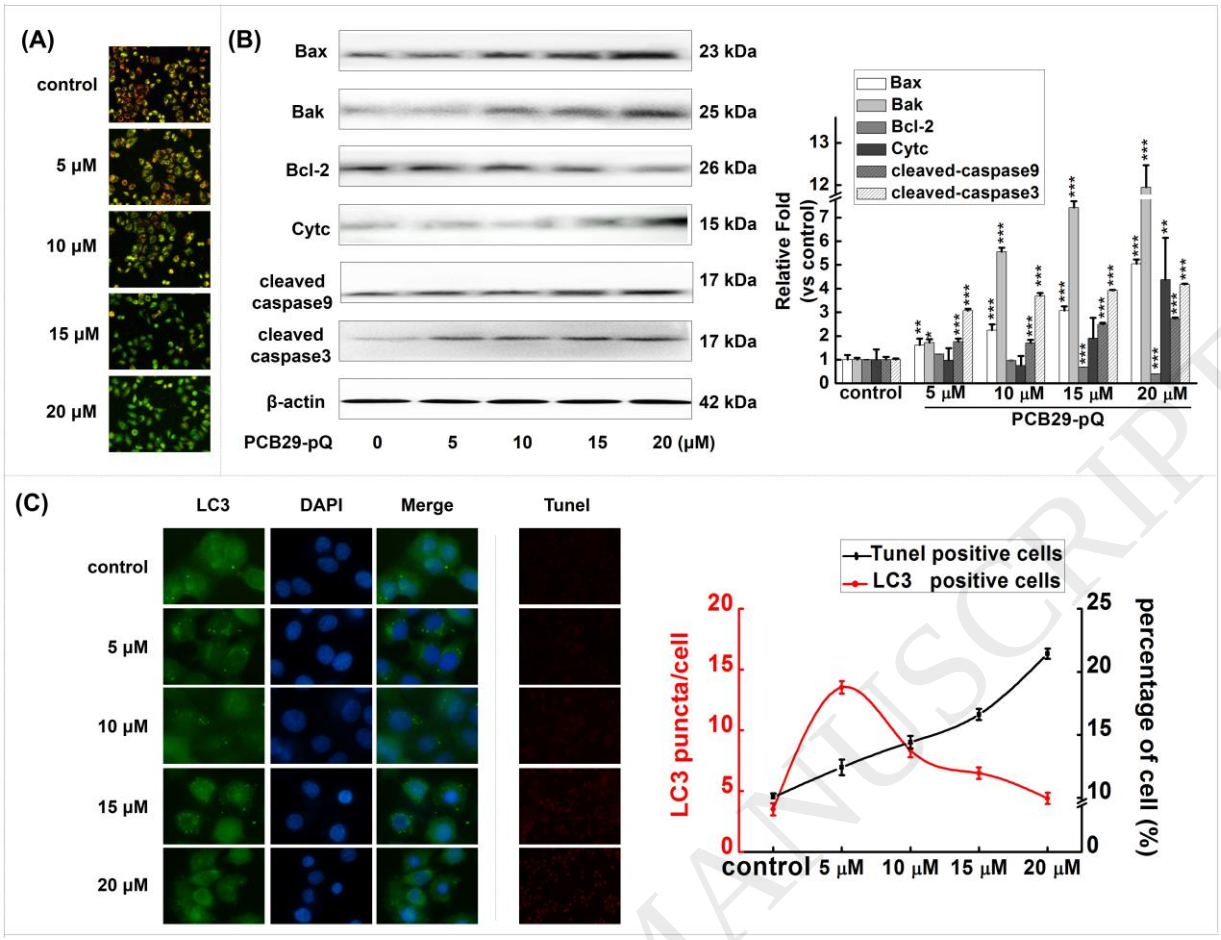

Figure 1. Autophagy-to-apoptosis signal switch via increasing the concentration of PCB29-pQ. HepG2 cells were treated with 5, 10, 15 or 20 μM PCB29-pQ for 24 h. (A) PCB29-pQ induced the loss of MMP. Images were captured with a fluorescence microscope. High membrane potential JC-1 forms orange fluorescence in control and lower concentration groups (5 and 10 μM), whereas lower membrane potential emits green fluorescence in higher concentration groups (15 and 20 μM). (B) Western blotting analysis of apoptosis-related protein expression, β-actin was used as the loading control. The data represent the mean ± SD of three independent experiments. *P<0.05, **P<0.01 and ***P<0.001 *vs* control group. (C) Immunofluorescence staining was performed to observe the expression of LC3 (green), nuclei stained with DAPI are shown in blue. The TUNEL assay was used to test apoptosis. Fluorescence analysis of images was performed with Image pro plus software, and the relative data are shown in the histogram.

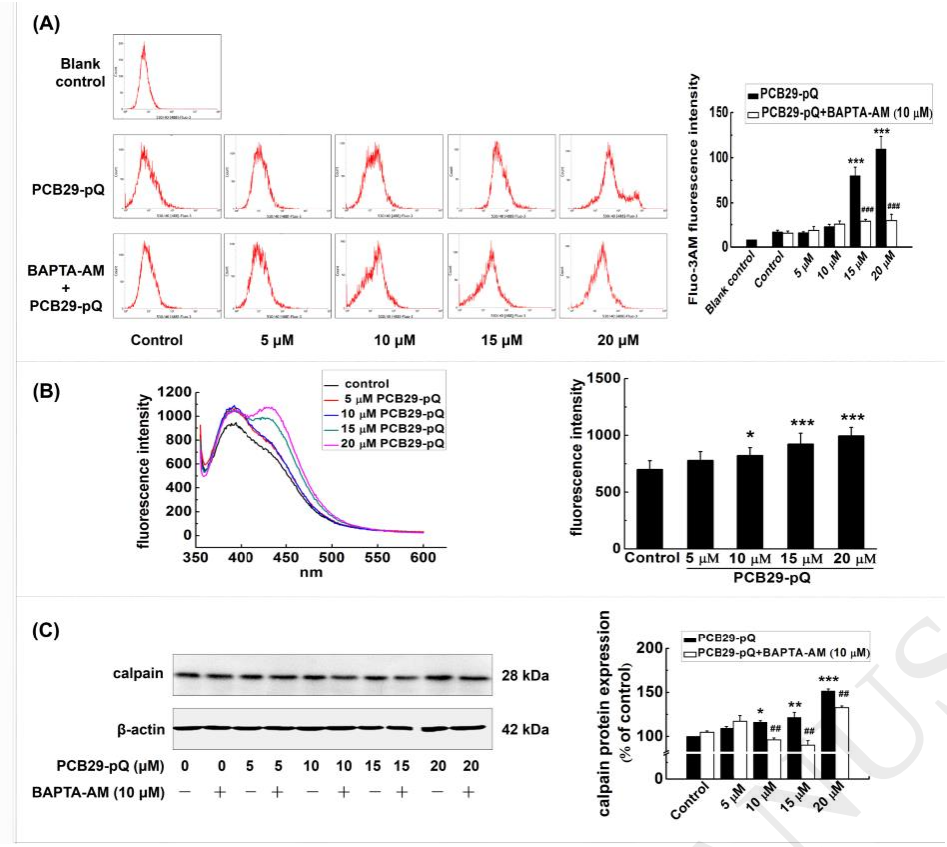

Figure 2. PCB29-pQ induced intracellular calcium levels and calpain activity in HepG2 cells. (A) HepG2 cells were incubated in the presence or absence of 10 μM BAPTA-AM for 1 h then treated with different concentrations of PCB29-pQ for 24 h. The intracellular calcium level of HepG2 cells was analyzed by flow cytometry. The relative fluorescence is shown in the histogram. (B) Calpain activity was determined by using S-LLVY-AMC as a cell-permeable fluorogenic calpain substrate. S-LLVY-AMC is cleaved by calpain to generate AMC. The AMC fluorescence intensity was measured with an excitation wavelength of 351 nm and an emission wavelength of 430 nm. The relative density of fluorescence is shown in the histogram. (C) HepG2 cells were incubated in the presence or absence of 10 μM BAPTA-AM for 1 h then treated with different concentrations of PCB29-pQ for 24 h. Western blot analysis of calpain protein expression. The data represent the mean ± SD of three independent experiments. *P<0.05, ***P<0.001 *vs* control, $^{###}$P<0.001 *vs* PCB29-pQ group.

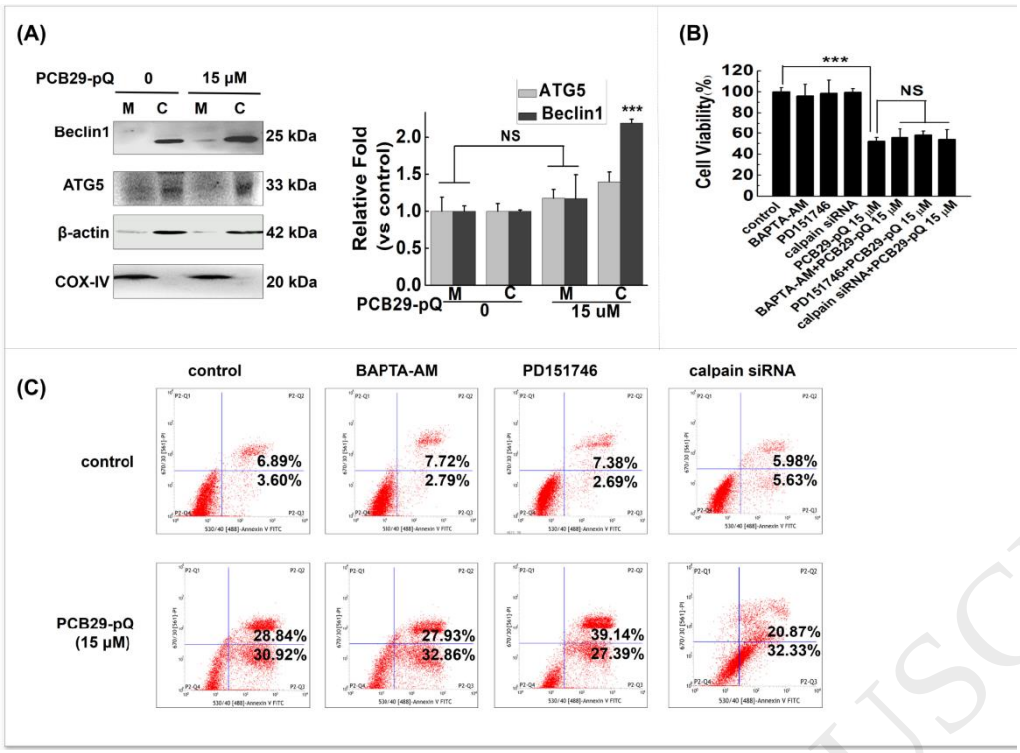

Figure 3. ATG5 and Beclin1 were cleaved with PCB29-pQ treatment. (A) HepG2 cells were treated with 15 μM PCB29-pQ for 24 h. Western blotting analysis of Beclin1 and ATG5 protein expression in mitochondria (M) and cytosol (C). β-actin and COX-IV were used as loading control for cytosol and mitochondria, respectively. (B) HepG2 cells were treated with calpain siRNA for 24 h. Cell viability of PCB29-pQ-treated HepG2 cells, with or without BAPTA-AM (Ca^{2+} chelator), PD151746 (calpain inhibitor) or calpain siRNA co-treatment for 24 h. The data represent the mean ± SD of three independent experiments. ***P< 0.001 vs control. NS, no significance. (C) HepG2 cells were treated with PCB29-pQ together with BAPTA-AM, PD151746 or calpain siRNA for 24 h. Flow cytometry analysis was performed with Annexin V-FITC and PI double-staining for apoptosis detection.

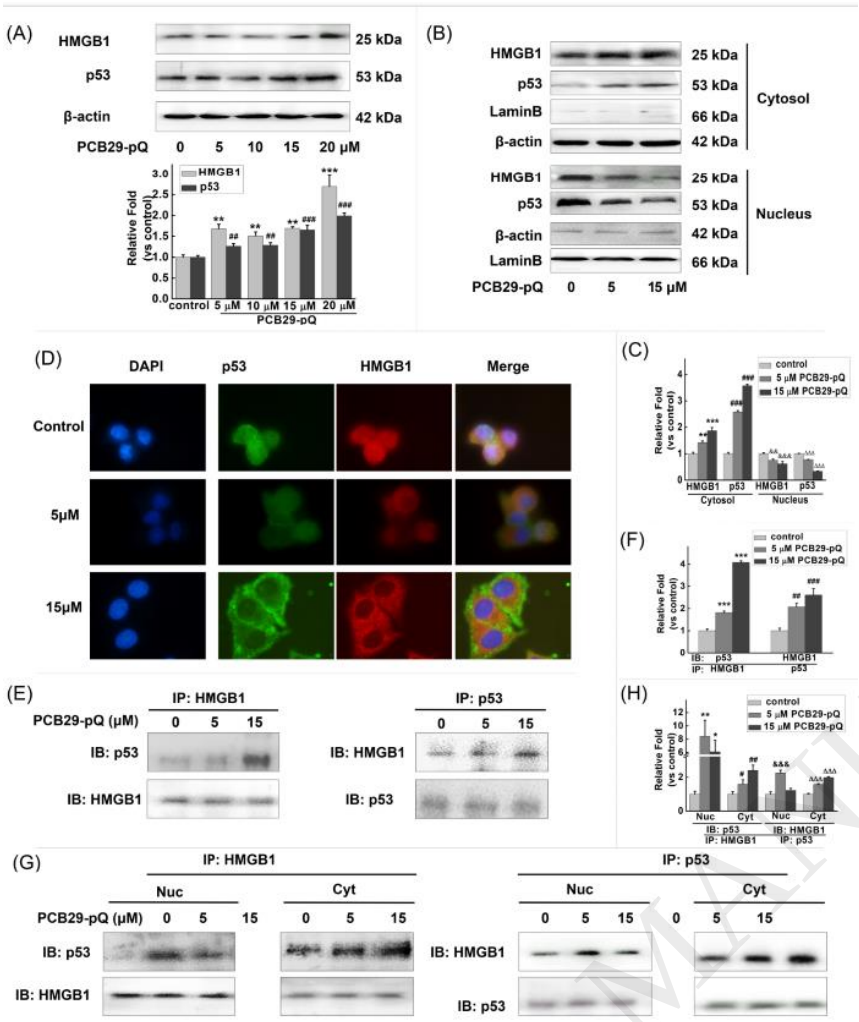

Figure 4. PCB29-pQ induced p53 and HMGB1 cytosolic translocation and the association between p53 and HMGB1 in HepG2 cells. (A) HepG2 cells were treated with 5, 10, 15 or 20 μM PCB29-pQ for 24 h. Western blotting analysis was performed, β-actin was used as the loading control. These protein expressions were shown in the histogram. The data represent the mean ± SD of three independent experiments. **P<0.01 and ***P<0.001 *vs* control (HMGB1), $^{\#\#}$P<0.01 and $^{\#\#\#}$P<0.001 *vs* control group (p53). (B-C) HepG2 cells were treated with 5 or 15 μM PCB29-pQ for 24 h. Western blotting analysis of p53 and HMGB1 protein expression in nucleus and cytosol. β-actin and Lamin B were used as loading control for cytosolic and nuclear fractions, respectively. p53 and HMGB1 protein expressions are shown in the histogram. The data represent the mean ± SD of three independent experiments. **P<0.01 and ***P<0.001 *vs* control (Cyt-HMGB1), $^{\#\#\#}$P<0.001 *vs* control

group (Cyt-p53). $^{\&\&}$P<0.01 and $^{\&\&\&}$P<0.001 *vs* control (Nuc-HMGB1), $^{\triangle\triangle\triangle}$P<0.001 *vs* control group (Nuc-p53). (D) HepG2 cells were treated with 5 or 15 μM PCB29-pQ for 24 h. Immunofluorescence staining was performed to observe the expression of p53 (green) and HMGB1 (red). Nuclei stained with DAPI are shown in blue. (E-F) HepG2 cells were treated with 5 or 15 μM PCB29-pQ for 24 h. The total proteins were extracted, immunoprecipitated with HMGB1 or p53 antibody, then precipitated proteins were analyzed by Western blotting with p53 or HMGB1 antibody. p53 and HMGB1 protein expressions are shown in the histogram. The data represent the mean ± SD of three independent experiments. ***P<0.001 *vs* control, $^{\#\#}$P<0.01 and $^{\#\#\#}$P<0.001 *vs* control group. (G-H) The nuclear and cytosolic proteins were extracted, immunoprecipitated with HMGB1 or p53 antibody, then precipitated proteins were analyzed by Western blotting with p53 or HMGB1 antibody. These protein expressions are shown in the histogram. The data represent the mean ± SD of three independent experiments. *P<0.05 and **P<0.01 *vs* control (Nuc-p53), $^{\#}$P<0.05 and $^{\#\#}$P<0.01 *vs* control group (Cyt-p53). $^{\&\&\&}$P<0.001 *vs* control (Nuc-HMGB1), $^{\triangle\triangle\triangle}$P<0.001 *vs* control group (Cyt-HMGB1).

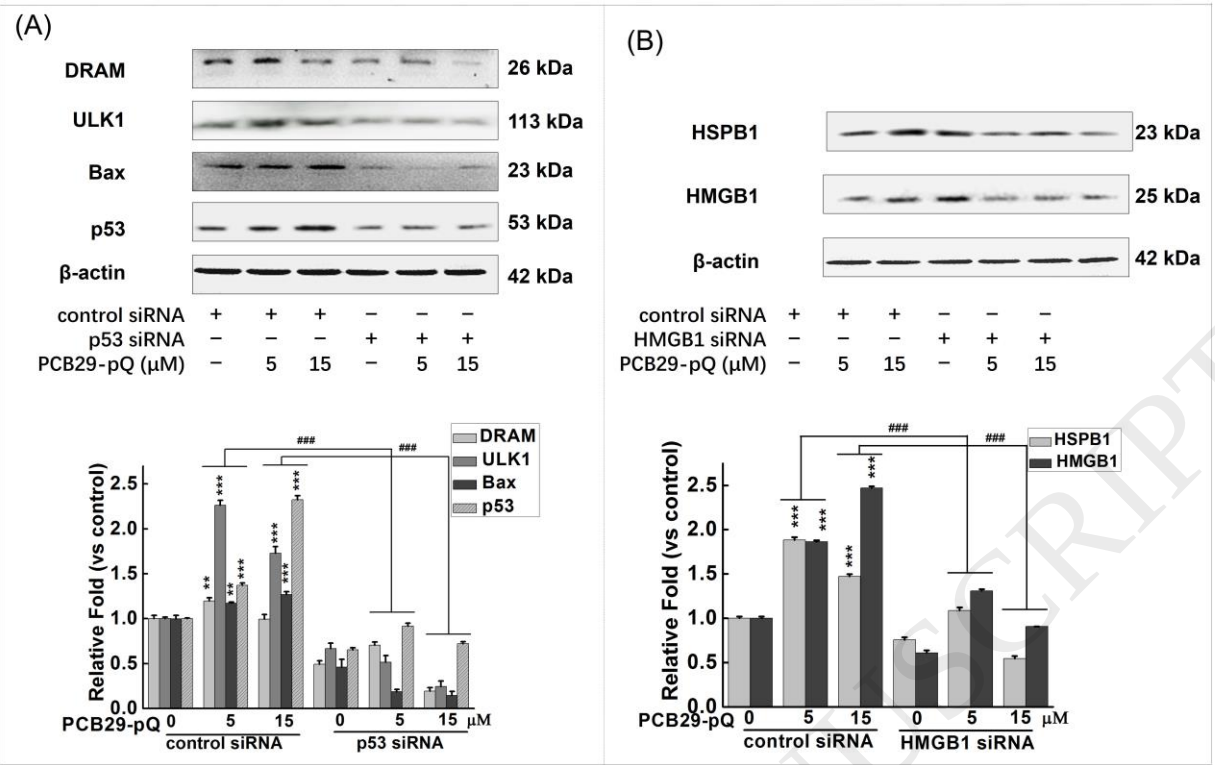

Figure 5. P53 and HMGB1 are linked to the regulation of autophagy and apoptosis as transcription factors. (A) HepG2 cells were pretreated with 50 nM p53 siRNA (or sham siRNA) for 24 h and exposed to 5 or 15 μM PCB29-pQ for an additional 24 h. Western blotting analysis was performed, β-actin was used as the loading control. These protein expressions were shown in the histogram. The data represent the mean ± SD of three independent experiments. **P<0.01 and ***P<0.001 *vs* control siRNA + 0 μM PCB29-pQ group, $^{\&}$P<0.05 and $^{\&\&\&}$P<0.001 was control siRNA + 15 μM PCB29-pQ *vs* control siRNA + 5 μM PCB29-pQ group, $^{\#\#\#}$P<0.001 *vs* control siRNA group. (B) HepG2 cells were pretreated with 50 nM HMGB1 siRNA (or sham siRNA) for 24 h and exposed to 5 or 15 μM PCB29-pQ for an additional 24 h. Western blotting analysis was performed, β-actin was used as the loading control. These protein expressions were shown in the histogram. The data represent the mean ± SD of three independent experiments. ***P<0.001 *vs* control siRNA + 0 μM PCB29-pQ group, $^{\&\&\&}$P<0.001 was control siRNA + 15 μM PCB29-pQ *vs* control siRNA + 5 μM PCB29-pQ group, $^{\#\#\#}$P<0.001 *vs* control siRNA group.

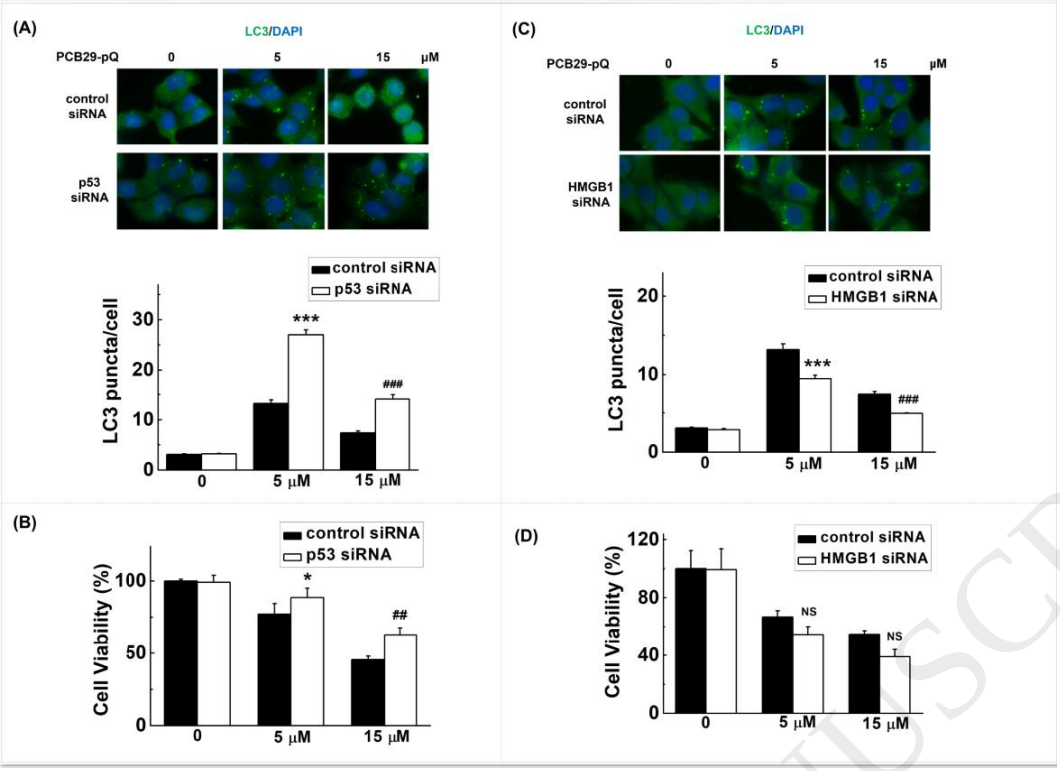

Figure 6. P53 and HMGB1 play different roles in autophagy and apoptosis in PCB29-pQ-treated cells. (A) HepG2 cells were pretreated with 50 nM p53 siRNA (or sham siRNA) for 24 h and exposed to 5 or 15 μM PCB29-pQ for an additional 24 h. Immunofluorescence staining was performed to observe the expression of LC3 (green), nuclei stained with DAPI are shown in blue. The relative fluorescence analysis was shown in the histogram. ***P<0.001 vs control siRNA + PCB29-pQ 5 μM group, $^{###}$P<0.001 vs control siRNA + PCB29-pQ 15 μM group. (B) HepG2 cells were pretreated with 50 nM p53 siRNA (or sham siRNA) for 24 h and exposed to 5 or 15 μM PCB29-pQ for an additional 24 h. Cell viability was assessed by CCK-8 test. The data represent the mean ± SD of three independent experiments. *P<0.05 vs control siRNA + PCB29-pQ 5 μM group, $^{##}$P<0.01 vs control siRNA + PCB29-pQ 15 μM group. (C) HepG2 cells were pretreated with 50 nM HMGB1 siRNA (or sham siRNA) for 24 h and exposed to 5 or 15 μM PCB29-pQ for an additional 24 h. Immunofluorescence staining was performed to observe the expression of LC3 (green), nuclei stained with DAPI are shown in blue. The relative fluorescence analysis was shown in the histogram.

***P<0.001 vs control siRNA + PCB29-pQ 5 μM group, ###P<0.001 vs control siRNA + PCB29-pQ 15 μM group. (D) HepG2 cells were pretreated with 50 nM HMGB1 siRNA (or sham siRNA) for 24 h and exposed to 5 or 15 μM PCB29-pQ for an additional 24 h. Cell viability was assessed by CCK-8 test. The data represent the mean ± SD of three independent experiments. NS, no significance, vs control siRNA + PCB29-pQ 5 μM group, or vs control siRNA + PCB29-pQ 15 μM group.